Accepted version. The final version is available at: DOI 10.1109/TMTT.2016.2623311

Splitter/Combiner Microstrip Sections Loaded with Pairs of Complementary Split Ring Resonators (CSRRs): Modeling and Optimization for Differential Sensing Applications

Lijuan Su, *Student Member IEEE*, Javier Mata-Contreras, Paris Vélez, *Member IEEE*, and Ferran Martín, *Fellow IEEE*

***Abstract*— This paper focuses on the analysis of splitter/combiner microstrip sections where each branch is loaded with a complementary split ring resonator (CSRR). The distance between CSRRs is high, and hence their coupling can be neglected. If the structure exhibits perfect symmetry with regard to the axial plane, a single transmission zero (notch) at the fundamental resonance of the CSRR, arises. Conversely, two notches (i.e., frequency splitting) appear if symmetry is disrupted, and their positions are determined not only by the characteristics of the CSRRs but also by the length of the splitter/combiner sections. A model that includes lumped elements (accounting for the CSRR-loaded line sections) and distributed components (corresponding to the transmission lines) is proposed and used to infer the position of the transmission zeros. Frequency splitting is useful for the implementation of differential sensors and comparators based on symmetry disruption. Using the model, the length of the splitter/combiner sections necessary to optimize the sensitivity of the structures as sensing elements is determined. Parameter extraction and comparison to electromagnetic simulations and measurements in several symmetric and asymmetric structures is used to validate the model. Finally, a prototype device sensor/comparator based on the proposed CSRR-loaded splitter/combiner microstrip sections is presented.**

***Index Terms*– Complementary split ring resonators (CSRRs), microstrip technology, circuit modeling, microwave sensors.**

I. Introduction

Many electromagnetic sensors are based on the variation of the resonance frequency, phase or quality factor of resonant elements, caused by the physical variable of interest (measurand) [1]-[18]. Among them, microwave sensors consisting of transmission lines loaded with planar resonators have been the subject of an intensive research activity in the last years [8],[9],[12],[18]. These structures are not exempt from a general drawback of sensors that limits their performance: cross sensitivity. Namely, the electrical variables are not only sensitive to the measurand, but also to other physical quantities. For instance, in resonance-based permittivity sensors, variations in temperature or moisture (environmental factors) may cause unintentional frequency shifts [15],[19], which in turn may produce systematic sensing errors. One solution to partially alleviate the effects of cross sensitivity, particularly those derived from changing environmental conditions, is differential sensing. Differential sensors are robust against variations in the ambient factors since such changes are seen as common-mode perturbations [16]-[18],[20],[21].

Differential sensors are typically implemented by means of two sensing elements, e.g., two loaded transmission lines, one of them acting as reference [16]. Nevertheless, it is possible to implement sensors scarcely sensitive to environmental factors by means of a single sensing element [22]-[24]. This can be achieved, for instance, by symmetrically loading a transmission line with a planar symmetric resonator [22],[25]-[32]. The sensing principle of these sensors is based on symmetry disruption. As pointed out in [22]-[24], by symmetrically loading a line with a resonator exhibiting symmetry plane of different electromagnetic nature (at the fundamental resonance) from the symmetry plane of the line (typically a magnetic wall, at least in microstrip or coplanar waveguide technology), the structure is transparent since coupling is prevented under these conditions. However, by truncating the symmetry, either electric or magnetic coupling (or both) between the line and the resonator may arise, with the result of a frequency notch (transmission zero) at the fundamental resonance frequency. Moreover, the magnitude of the notch (related to the coupling level) is determined by the level of asymmetry. Note, however, that in these coupling-modulated resonance sensors [24], environmental conditions do not produce misalignment between the line and the resonator or any other type of symmetry disruption. Therefore, these sensors are similar to differential sensors in terms of robustness against environmental factors.

Another type of sensors also exhibiting small cross sensitivity to environmental conditions is based on the symmetric loading (or coupling) of a transmission line with a pair of resonant elements [33]-[38]. Such sensors, referred to as frequency-splitting sensors [24], are true differential sensors with two sensing elements (the resonators). In this case, the sensing principle is also related to symmetry, but different than the one for coupling-modulated resonance sensors. In brief, under perfect symmetry, the structure exhibits a single transmission zero (provided the resonant elements are coupled to the line or in contact with it); however, by truncating symmetry, e.g., by loading the

This paper is an expanded version from the 2016 International Microwave Conference, San Francisco, CA, May 22-27, 2016. This work was supported by MINECO-Spain (project TEC2013-40600-R), *Generalitat de Catalunya* (project 2014SGR-157), *Institució Catalana de Recerca i Estudis Avançats* (who awarded Ferran Martín), and by FEDER funds. Lijuan Su acknowledges the China Scholarship Council (CSC) for the grant 201306950011.

The authors are with GEMMA/CIMITEC, Departament d'Enginyeria Electrònica, Universitat Autònoma de Barcelona, 08193 Bellaterra, Spain. E-mail: Ferran.Martin@uab.es.

resonators with unbalanced dielectric loads, two notches arise, and the frequency difference depends on the level of asymmetry. One limitation of these frequency-splitting sensors may be caused by the possible coupling between resonant elements (unavoidable if such elements are close enough). Such coupling, if present, severely degrades the sensitivity for small perturbations [34]. Inter-resonator coupling can be prevented by considering two resonant elements separated enough, each one coupled to (or in contact with) a different transmission line in a splitter/combiner configuration as the one proposed in [39] (an alternative is a cascaded configuration, as reported in [40], where the authors consider stepped impedance resonators). However, in this case, the sensitivity is degraded by the length of the lines, and sensing, also related to symmetry disruption and based on the separation between transmission zeros (the output variable), is influenced by the interference between the pair of resonator-loaded lines. In other words, the transmission zeros are not only dictated by the intrinsic resonance frequency of the resonators, but also by the length of the lines, and such transmission zeros occur, in general, at those frequencies where the signals at the end of each loaded line exactly cancel.

This paper is focused on the analysis of frequency-splitting sensors based on splitter/combiner microstrip sections loaded with complementary split ring resonators (CSRRs), first presented in [39]. The main aim is to optimize the sensitivity to unbalanced loads or, more specifically, to obtain the necessary conditions (length of the splitter/combiner sections) to achieve such optimization. The analysis, based on a mixed distributed/lumped model of the considered structures is presented in Section II. This section, supported by the two appendixes, constitutes the main contribution of the paper, as compared to [39]. It is clearly pointed out that one of the transmission zeros may be given by the resonance of the CSRRs, if a suitable electrical length between the position of the CSRR and the T junctions is chosen. Validation of the model, including sensitivity optimization, is discussed in Section III, where it is clearly pointed out that sensitivity is optimized if such electrical length is selected. In Section IV, a prototype device acting as a differential sensor and comparator, i.e., a device able to detect differences between a sample under test (SUT) and a reference sample and useful for differential measurements of dielectric constant, is presented (this includes measurement of the dielectric constant of a known substrate –to demonstrate the potential of the approach– and estimation of the effective dielectric constant of a sample with defects). Finally, the main conclusions are highlighted in section V.

II. TOPOLOGY, CIRCUIT MODEL AND ANALYSIS

The typical topology (including relevant dimensions) of the considered power splitter/combiner microstrip structure with CSRRs etched in the ground plane is shown in Fig. 1(a). Each branch consists of a 50 Ω line loaded with a CSRR, etched in the ground plane. To match the structure to the 50 Ω ports, impedance inverters implemented by means of 35.35 Ω quarter wavelength transmission line sections are cascaded between the ports and the T-junctions. The circuit schematic, with distributed and lumped elements, is shown in Fig. 1(b). An asymmetric structure is considered as general case, but asymmetry refers to the dimensions of the CSRR, rather than the transmission line sections. The lumped elements account for the CSRR-loaded microstrip line sections. Thus, L_u (L_l) and C_u (C_l) model the inductance and capacitance of the microstrip line, respectively, above the CSRR in the upper (lower) parallel branch, and the resonators (CSRRs) are accounted for by the tanks L_{Cu}-C_{Cu} (upper CSRR) and L_{Cl}-C_{Cl} (lower CSRR) [41]. The distributed elements account for the transmission line sections which are not located on top of the CSRRs. The line impedance Z_i and the electrical length θ_i (with i = 1,2) define such line sections.

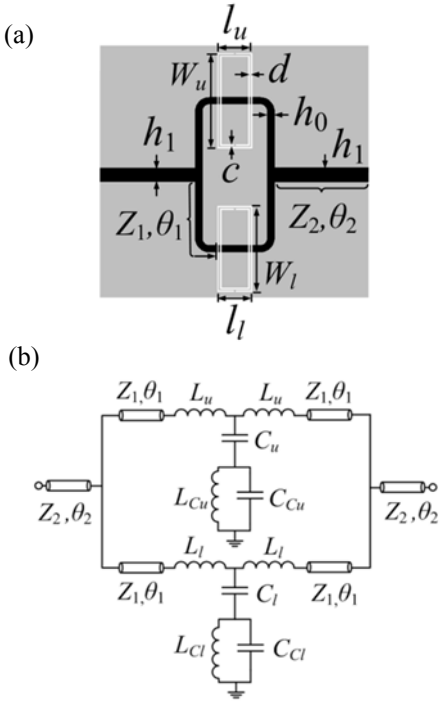

Fig. 1. (a) Typical topology of the power splitter/combiner loaded with two CSRRs and (b) circuit schematic.

Note that to predict the transmission zero frequencies through the schematic of Fig. 1(b), the input and output transmission line sections can be neglected (such sections do not have influence on the position of the notches). The two-port network then contains two parallel branches. Thus, for analysis purposes, it is convenient to deal with the admittance matrix. Let us now center on the two-port network of Fig. 2, where the output port is terminated with the reference impedance Z_0. A transmission zero (i.e., total reflection) results if the current at the output port is zero (I_2 = 0) and $I_1 \neq 0$. From the admittance matrix equation, considering the indicated load at port 2, the following results are obtained:

$$I_1 = Y_{11}V_1 + Y_{12}Z_0 I_2 \tag{1a}$$

$$I_2 = Y_{21}V_1 + Y_{22}Z_0 I_2 \tag{1b}$$

and from these equations, I_2 can be isolated, that is

$$I_2 = \frac{Y_{21}}{Y_{11}(1 - Y_{22}Z_0) + Y_{21}Y_{12}Z_0} I_1 \tag{2}$$

Therefore, $Y_{21} = 0$ with the denominator of (2) different than zero), or $Y_{11} = \infty$ with $Y_{21} \neq \infty$ are sufficient conditions to obtain a transmission zero. It follows from reciprocity that $Y_{12} = 0$, or $Y_{22} = \infty$ are also sufficient conditions to obtain total reflection. Indeed, since the considered structure is symmetric with regard to the mid-plane between the input and output ports, the transmission zero frequencies should simply satisfy $Y_{21} = Y_{12} = 0$, and/or $Y_{11} = Y_{22} = \infty$.

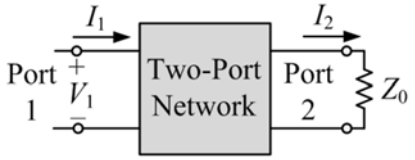

Fig. 2. Two-port network loaded with the impedance Z_0 at the output port.

Let us distinguish the anti-diagonal elements of the admittance matrices of the upper and lower branches of the structure of Fig. 1 by the sub-indexes *u* and *l*. Thus, Y_{21} is given by

$$Y_{21} = Y_{21,u} + Y_{21,l} \tag{3}$$

and $Y_{21,u}$ and $Y_{21,l}$ can be determined by first obtaining the *ABCD* matrix of each branch. This is given by the matrix product of the matrices corresponding to the three cascaded two-port networks, that is, the pair of transmission line sections with characteristic impedance Z_1, and the sandwiched lumped two-port network. From the *ABCD* matrices for each branch, the elements of the right-hand side in (3) are given by $Y_{21,u} = -1/B_u$ and $Y_{21,l} = -1/B_l$, where B_u and B_l are the *B* elements of the *ABCD* matrix for the upper and lower branches, respectively [42]. Thus, the transmission zeros related to $Y_{21} = Y_{12} = 0$ are given by:

$$\frac{1}{B_u} + \frac{1}{B_l} = 0 \tag{4}$$

with

$$B_u = j(Z_1 \sin 2\theta_1 + 2\omega L_u \cos^2\theta_1) + j\frac{\left(Z_1 \sin\theta_1 + \omega L_u \cos\theta_1\right)^2}{\dfrac{\omega L_{Cu}}{1-\dfrac{\omega^2}{\omega_{Cu}^2}} - \dfrac{1}{\omega C_u}} \tag{5a}$$

$$B_l = j(Z_1 \sin 2\theta_1 + 2\omega L_l \cos^2\theta_1) + j\frac{\left(Z_1 \sin\theta_1 + \omega L_l \cos\theta_1\right)^2}{\dfrac{\omega L_{Cl}}{1-\dfrac{\omega^2}{\omega_{Cl}^2}} - \dfrac{1}{\omega C_l}} \tag{5b}$$

with $\omega_{Cu} = (L_{Cu} \cdot C_{Cu})^{-1/2}$ and $\omega_{Cl} = (L_{Cl} \cdot C_{Cl})^{-1/2}$. The general solution of (4) is not simple. However, it is possible to obtain the pair of transmission zeros numerically. Also, we can obtain the influence of the element values on the position of such transmission zeros. Particularly, the effects of the asymmetry produced by the CSRRs can be studied. If two identical CSRRs are considered, (4) gives a unique solution (transmission zero) with angular frequency given by

$$\omega_z = \frac{1}{\sqrt{L_r (C_r + C)}} \tag{6}$$

where $L_{Cu} = L_{Cl} = L_r$, $C_{Cu} = C_{Cl} = C_r$, and $C_u = C_l = C$. Note that (6) is the frequency that shorts to ground the reactance of the identical shunt branches of the lumped two-port T-networks of Fig. 1(b), as expected.

Except for the symmetric case, where the single transmission zero is simply given by the characteristics of the resonators and their coupling to the line, the two transmission zeros of the general case are consequence of an interfering phenomenon between the parallel CSRR-loaded line sections.

Let us now consider the alternative situation providing transmission zeros, that is, $Y_{11} = Y_{22} = \infty$ with $Y_{21} = Y_{12} \neq \infty$. In this case, we can analyze each branch independently. The reason is that $Y_{11,u} = \infty$ and/or $Y_{11,l} = \infty$ (where the sub-indexes *u* and *l* have been defined before) suffices to guarantee that $Y_{11} = Y_{11,u} + Y_{11,l} = \infty$. Therefore, let us calculate, e.g., $Y_{11,u}$. This parameter can be inferred from the elements of the *ABCD* matrix as $Y_{11,u} = D_u/B_u$ [42]. Even though B_u has been calculated before, this element can be simplified by designating by Y_u the admittance of the shunt branch (formed by C_u, L_{cu}, C_{cu}). We can proceed similarly in order to calculate D_u. Once B_u and D_u have been inferred, $Y_{11,u}$ can be expressed as a function of Y_u, i.e.,

$$Y_{11,u} = \frac{\cos 2\theta_1 - \dfrac{\omega L_u}{Z_1}\sin 2\theta_1 + jY_u\left(\omega L_u \cos 2\theta_1 + Z_1 \dfrac{\sin 2\theta_1}{2} - \omega^2 L_u^2 \dfrac{\sin 2\theta_1}{2Z_1}\right)}{j\left(2\omega L_u \cos^2\theta_1 + Z_1 \sin 2\theta_1\right) - Y_u\left(Z_1 \sin\theta_1 + \omega L_u \cos\theta_1\right)^2} \tag{7}$$

Inspection of (7) reveals that $Y_u = \infty$ (corresponding to a short circuit) may provide $Y_{11,u} = \infty$. However, this is not a sufficient condition. To verify this, let us calculate $Y_{11,u}$ in the limit when $Y_u \to \infty$. The result is as follows:

$$Y_{11,u} = -j\frac{\left(\omega L_u \cos 2\theta_1 + Z_1 \dfrac{\sin 2\theta_1}{2} - \omega^2 L_u^2 \dfrac{\sin 2\theta_1}{2Z_1}\right)}{\left(Z_1 \sin\theta_1 + \omega L_u \cos\theta_1\right)^2} \tag{8}$$

and this result is in general finite, unless the following condition is satisfied

$$Z_1 \sin\theta_1 + \omega_0 L_u \cos\theta_1 = 0 \tag{9}$$

In (9), ω_0 is the frequency where $Y_u = \infty$. From (9), the following result is inferred

$$\theta_1 = \arctan\left(-\frac{\omega_0 L_u}{Z_1}\right) = \pi - \arctan\left(\frac{\omega_0 L_u}{Z_1}\right) \equiv \theta_{1,\infty} \tag{10}$$

(10) gives the electrical length at ω_0 that is necessary to obtain $Y_{11,u} = \infty$ and hence $Y_{11} = \infty$. However, note that in view of (2), $Y_{11} = \infty$ does not guarantee $I_2 = 0$, as required to obtain a transmission zero. We can however express (2), for the upper branch, in terms of the *ABCD* matrix as follows:

$$I_2 = \frac{B_u}{D_u B_u - D_u^2 Z_0 + Z_0} I_1 \tag{11}$$

With the condition (9), $B_u = 0$ and $D \neq 1$ (see Appendix I). Therefore, it is demonstrated that $Y_u = \infty$ and (9) are sufficient conditions to obtain a transmission zero.

The physical interpretation of this transmission zero is very clear. The solution of θ_1 provided by (9) corresponds to the electrical length of the line necessary to translate the shunt branch to the input or output port. Note that if $L_u = 0$, such electrical length is simply $\theta_1 = \pi$, as expected. Thus, if the frequency that nulls the reactance of the shunt branch satisfies (9), a short is present in the input and output ports of the upper branch, hence providing a transmission zero to the whole structure. Note that such transmission zero frequency does not depend on the characteristics of the other (lower) branch, and hence it is not associated to an interfering phenomenon, contrary to the other transmission zero (assuming asymmetry) which is still related to the destructive interference of the two branches.

It is interesting to mention that since condition (9) translates to the input and output ports the shunt reactance, such condition should also be derived by forcing the electrical length of the whole upper branch to be 2π (by excluding the shunt reactance and by considering this branch as the unit cell of a periodic structure). This is demonstrated in Appendix II.

III. Model Validation and Optimization for Sensing Purposes

Model validation has been carried out by comparing lossless electromagnetic simulations of different structures with circuit simulations. To this end, it has been necessary to extract the circuit elements describing the transmission line sections loaded with CSRRs following the procedure described in [43]. For that purpose, we have first independently simulated the considered CSRR-loaded microstrip sections.

We have first considered the symmetric CSRR-loaded splitter/combiner section as depicted in Fig. 1(a). The frequency response (magnitude of the transmission coefficient) inferred from electromagnetic simulation, using the *Keysight Momentum* commercial software, is depicted in Fig. 3(a). This figure also depicts the response resulting from circuit simulation by using the extracted element values, indicated in the caption. Then, we have considered two asymmetric structures where we have modified only the dimensions of the lower CSRR, specifically W_l, by increasing or decreasing ΔW_l, leaving the upper CSRR unaltered. In one case this dimension has been increased and in the other one it has been decreased. The responses (electromagnetic and circuit simulations) are depicted in Figs. 3(b) and (c), where the corresponding sets of extracted parameters are indicated (see caption). In all the cases, there is very good agreement between the electromagnetic and circuit simulations, pointing out the validity of the model. Fig. 3 also includes the measured responses, inferred from the *Agilent N5221A* vector network analyzer [see the picture of the experimental set-up in Fig. 3(d)].

We have carried out further electromagnetic simulations with different values of W_l. The pairs of transmission zeros as a function of $\Delta W_l/W_l$ are depicted in Fig. 4(a). As ΔW_l tends to be zero, corresponding to the symmetric structure, the separation between the transmission zeros decreases. However, it can be appreciated in Fig. 4(a) that both transmission zeros do not converge (a sudden jump occurs when the structure is symmetric, with only one transmission zero, as anticipated before).

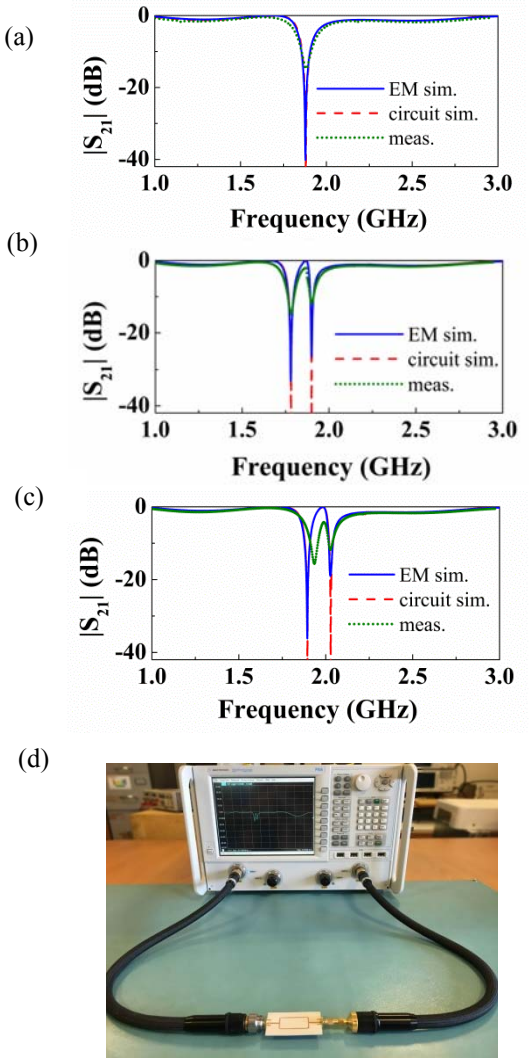

Fig. 3. (a) Magnitude of the transmission coefficient corresponding to the symmetric structure of Fig 1(a) by considering the *Rogers RO3010* substrate with thickness $h = 1.27$ mm and dielectric constant $\varepsilon_r = 10.2$, and with geometrical parameters as follows: h_0=1.15 mm, h_1=2.22 mm, $c = 0.2$ mm, $d = 0.2$ mm, $W_u = W_l = 7.86$ mm, $l_u = l_l = 4.8$ mm; (b) Magnitude of the transmission coefficient obtained by increasing the length of the lower CSRR with $\Delta W_l = 0.1W_u = 0.786$ mm; (c) Magnitude of the transmission coefficient obtained by decreasing the length of the lower CSRR with $\Delta W_l = -0.1W_u = -0.786$ mm; (d) Photograph of the experimental set-up. The extracted parameters are: (a) $L_u = L_l = 2.18$ nH, $C_u = C_l = 0.82$ pF, $L_{Cu} = L_{Cl} = 1.91$ nH, and $C_{Cu} = C_{Cl} = 2.94$ pF; (b) $L_l = 2.30$ nH, $C_l = 0.82$ pF, $L_{Cl} = 2.08$ nH, and $C_{Cl} = 3.09$ pF; (c) $L_l = 2.07$ nH, $C_l = 0.82$ pF, $L_{Cl} = 1.70$ nH, and $C_{Cl} = 2.84$ pF. For both (b) and (c), the rest of extracted element values are the same as (a).

In the structure of Fig. 1(a), giving the responses of Fig. 3 and the pairs of transmission zeros of Fig. 4(a) for different values of W_l, the electrical length of the transmission line sections between the T-junctions and the position of the CSRRs, θ_l, does not satisfy (10). Particularly, in Fig. 1(a) $\theta_1 < \theta_{1,\infty}$, where $\theta_{1,\infty}$ is the phase that satisfies (10). We have repeated the electromagnetic simulations of the structures considered in Fig. 4(a), but by considering $\theta_1 > \theta_{1,\infty}$. The pairs of transmission zeros that result by varying W_l are depicted in Fig. 4(b). The behaviour is very similar to the one observed in Fig. 4(a). However, the single transmission zero for the symmetric structure belongs now to the opposite curve.

Finally, we have considered the case with $\theta_l = \theta_{l,\infty}$ [Fig. 4(c)]. In this case, the pair of transmission zeros merge when the structure is symmetric, and the two curves cross. This is an expected result since it was demonstrated in the previous section that when condition (10) is satisfied one of the transmission zeros is given by the frequency that nulls the reactance of the upper shunt branch, regardless of the dimensions of the CSRR present at the other (lower) branch. Concerning the frequency response, a typical characteristic when $\theta_l = \theta_{l,\infty}$ is the similarity between the two notches (depth and width) for asymmetric structures, as it can be appreciated in Fig. 5.

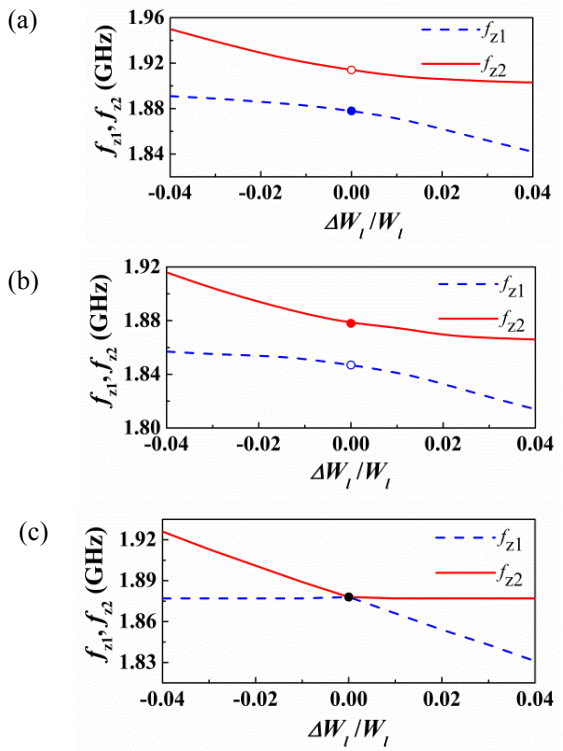

Fig. 4. Variation of the transmission zeros as a function of the variation of the width of one of the CSRRs ($\Delta W_l/W_l$) for different electrical lengths of the transmission lines: (a) $\theta_l = 0.672\pi < \theta_{l,\infty}$; (b) $\theta_l = 1.008\pi > \theta_{l,\infty}$; (c) $\theta_l = 0.84\pi = \theta_{l,\infty}$.

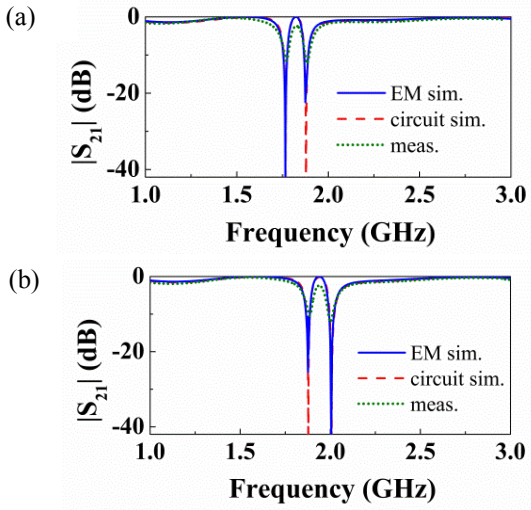

Fig. 5. Response of the CSRR-loaded combiner/splitter structure with $\theta_l = \theta_{l,\infty}$ for two asymmetric structures. (a) $W_l = 8.65$ mm, by increasing $\Delta W_l = 0.1$ $W_u = 0.786$ mm; (b) $W_l = 7.07$ mm, by decreasing $-\Delta W_l = -0.1$ $W_u = -0.786$ mm.

If we use the CSRR-loaded splitter/combiner structures as sensors or comparators based on frequency splitting, where the sensitivity is defined as the variation of the frequency difference between the two transmission zeros (f_{z1} and f_{z2}) with the variable that generates the asymmetry (typically a difference in dielectric constant between two samples), it follows that the optimum structure in terms of sensitivity is the one satisfying (10), i.e., the one giving the transmission zeros of Fig. 4(c). In Fig. 4, the asymmetries are caused by varying the dimensions of one of the CSRRs, but this behaviour (the dependence of the transmission zero curves with θ_l) does not depend on the cause of the asymmetry, and it is general for unbalanced loads. Thus, without loss of generality, we can define the sensitivity as

$$S = \frac{\partial \Delta f_z}{\partial \Delta W_l} \tag{12}$$

where $\Delta f_z = f_{z1} - f_{z2}$. The sensitivity for the three considered cases is depicted in Fig. 6, where it can be appreciated that the sensitivity for small unbalanced perturbations is clearly optimized when $\theta_l = \theta_{l,\infty}$ (note that if the optimum electrical length, 0.84π in our case, is not considered, but it is very close to this value, the sensitivity is expected to approach the optimum value for practical unbalanced loads).

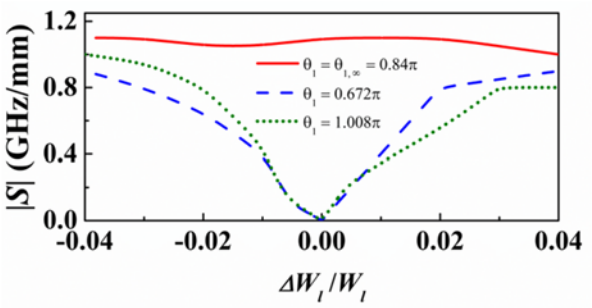

Fig. 6. Sensitivity as a function of $\Delta W_l/W_l$ for different values of the electrical length of the transmission lines.

IV. PROTOTYPE DEVICE SENSOR AND COMPARATOR

To demonstrate the potential of the structure with $\theta_l = \theta_{l,\infty}$ as sensor and comparator, we have first loaded it (i.e., the lower CSRR, acting as the active sensor region) with small dielectric slabs with different dielectric constant (the other CSRR is kept unloaded). Specifically, we have cut square-shaped pieces of un-metalized commercial microwave substrates with dielectric constants of 10.2 (*Rogers RO3010*), 3.55 (*Rogers RO4003C*) and 2.43 (*Arlon CuClad 250*). The measured responses are depicted in Fig. 7(a), whereas the variation of frequency splitting, Δf_z, with the dielectric constant, exhibiting roughly a linear variation, is shown in Fig. 7(b). This curve can be used to determine the dielectric constant of unknown substrates/samples from the measurement of the resulting frequency splitting. The dielectric constant of the SUT can in principle be arbitrarily small. Nevertheless, as the dielectric constant of the sample approaches unity, the two notches may merge in a single one by the effect of losses of the device (metallic and dielectric). Therefore, the discrimination is limited by this effect. Considering SUTs with large dielectric constant would force us to consider additional samples with known large dielectric constant in order to extend the span of the calibration curve. Apart from that, the curve of Fig. 7(b)

reveals a significant variation of Δf_z with the dielectric constant. If we assume that frequency differences (for different samples) of the order of 0.01 GHz can be distinguished (reasonable on account of the peaked responses at the notches), then differences in dielectric constants of the order of 0.35 or even less, can be detected.

As a test example, we have loaded the device with a square slab of un-cladded *FR4* substrate (with nominal dielectric constant 4.5). The resulting frequency splitting is Δf_z = 0.112 GHz, providing a dielectric constant of 4.56, according to the curve of Fig. 7(b), i.e., in close agreement to the nominal value.

It is worth mentioning that the SUT is assumed to be a dielectric slab larger than the dimensions of the CSRRs. The relative position of the SUT with regard to the CSRR is not relevant as long as the SUT limits are beyond those of the CSRRs. Otherwise, the notch frequency will depend on the relative position between the SUT and the CSRR, situation that must be avoided. In principle, the proposed sensor system is useful for dielectric slabs, not for samples with arbitrary geometry. The reason is that the CSRR slots must be surrounded by the SUT material under consideration. Concerning the potentiality of this approach for the characterization of the dielectric constant of liquids, the system may be useful as long as the experimental set up is able to guarantee sealing. Obviously this needs further work, which is out of the scope of this paper. The main aim of the paper is the determination of the dielectric constant in low-loss dielectric samples.

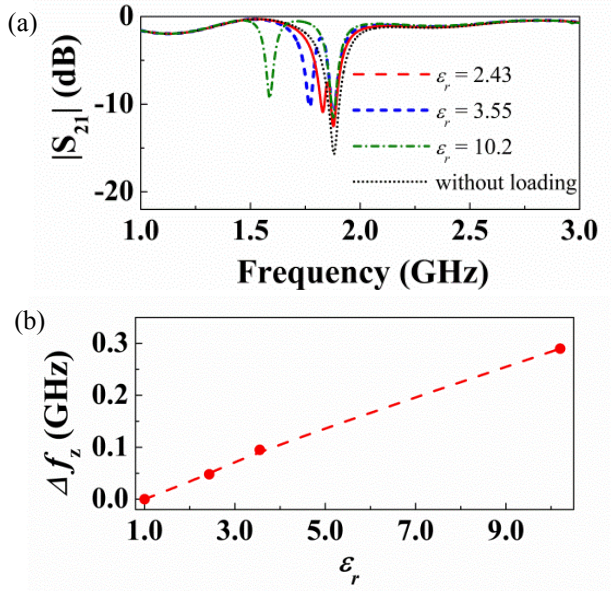

Fig. 7. (a) Response of the CSRR-loaded combiner/splitter structure with $\theta_1 = \theta_{1,\infty}$ to different dielectric loads and (b) variation of Δf_z with the dielectric constant of the considered load.

To demonstrate its use as comparator, we have loaded the structure with two square-shaped pieces of un-metalized *Rogers RO3010* substrate (with dielectric constant 10.2), but with defects in one of the samples (the SUT) in the form of a square array of vertical cylindrical holes with radius 0.2 mm and separated 0.8 mm (see Fig. 8). This reduces the effective dielectric constant. The measured response (Fig. 9) gives two notches, indicative of the difference between the two samples, the SUT and the reference sample (unaltered piece of substrate).

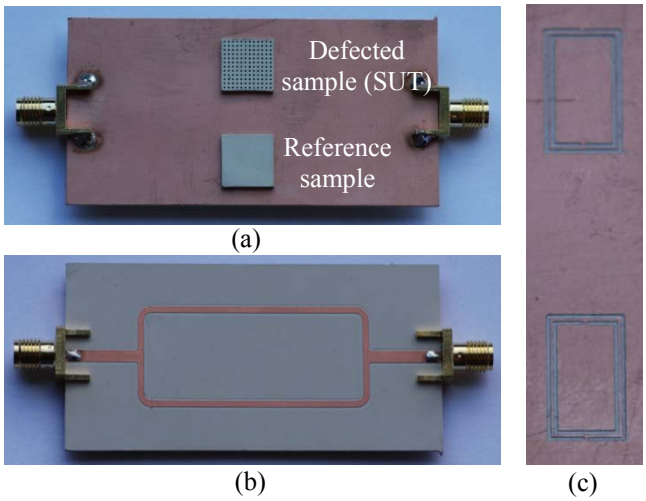

Fig. 8. Photograph of the splitter/combiner loaded with the reference sample and the SUT. (a) Bottom view; (b) top view. The detail of the CSRRs, not shown in (a) by the presence of the slabs, is shown in (c).

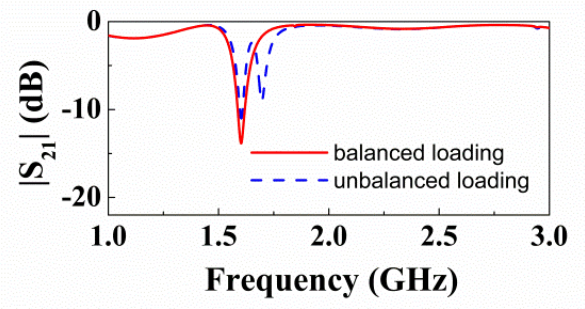

Fig. 9. Response of the CSRR-loaded combiner/splitter structure to two unbalanced loads, i.e., a reference sample and the same sample with defects (SUT). The response with both CSRRs loaded with the reference sample (balanced loading) is also included for comparison.

The SUT has been also measured with the other CSRR unloaded (similar to the experiment carried out in Fig. 7). The resulting frequency splitting, Δf_z = 0.204 GHz, indicates that the effective dielectric constant of the sample is in the vicinity of 7.4, according to the curve in Fig. 7(b). This is a reasonable value on account of the perforated cylindrical holes across the sample.

Another interesting aspect concerns the effects of pressure applied to the SUT, related to the presence of an air gap between the CSRRs and the samples. In our case, we have simply left the samples to rest on top of the CSRRs. By putting pressure, the notch positions certainly change. However, the device will work both as sensor and as comparator as long as the pressure is the same in the SUT and reference sample (comparator), or in the considered SUT as compared to the samples used for calibration (sensor).

V. CONCLUSIONS

In conclusion, splitter/combiner microstrip sections loaded with pairs of CSRRs have been studied in detail. These structures are useful as sensors and comparators, and their working principle is based on frequency splitting caused by symmetry disruption on the CSRR pair. Thus, the structures are especially suitable for the measurement of the dielectric constant of samples (sensor functionality) and for the detection of defects or anomalies in a sample under test, as compared to a reference sample (comparator functionality). We have proposed a mixed

distributed/lumped circuit model of the structures, which has been validated by comparison between the circuit responses obtained from circuit simulation (with extracted parameters) and those inferred from electromagnetic simulation and experiment. From the circuit model, we have obtained the necessary conditions, relative to the electrical length of the transmission line sections of the splitter/combiner, to optimize the sensitivity of the structures as sensing elements and the discrimination as comparators. Finally, we have demonstrated the potential of the reported CSRR-based structures as sensors and comparators by considering different dielectric loads, located in the active region of the sensor (one of the CSRRs), and by obtaining the resulting frequency splitting, and by comparing a defected sample under test (SUT) with a reference (unaltered) sample. In the latter case, the presence of two notches in the frequency response indicates the difference between the two samples. The reported approach solves the limitation of previous sensing structures based on pairs of CSRRs loading a single line, where coupling between resonators degrades the sensitivity and discrimination. As pointed out in [39], several samples can be sensed/compared simultaneously by cascading several splitter/combiner sections, each one loaded with a different pair of CSRRs. Nevertheless, up to three samples can be also measured with a single splitter/combiner, by adequately locating three pairs of CSRRs in the structure: two of them in the input/output access lines, two of them in the parallel microstrip lines, at a distance given by (10) from the input T-junction, and the remaining two CSRRs also in the parallel microstrip lines at a distance given by (10) from the T-junction adjacent to the output port.

APPENDIX I

B_u, the denominator of (7), can be expressed as

$$B_u = j2\cos\theta_1\left(\omega L_u\cos\theta_1 + Z_1\sin\theta_1\right) - \\ - Y_u\left(Z_1\sin\theta_1 + \omega L_u\cos\theta_1\right)^2 \qquad \text{(AI.1)}$$

Since the condition (9) is a common factor in the previous equation, it follows that $B_u = 0$ if (9) is satisfied. Actually, from a mathematical viewpoint, the second term in the right-hand side can be null, infinite or finite, depending on the variation of Y_u with frequency in the limit when $\omega \to \omega_0$. However, for any shunt admittance, Y_u, it can be demonstrated that such term is null. To this end, let us calculate this term in the indicated limit, i.e.,

$$\lim_{\omega\to\omega_0}\frac{\left(Z_1\sin\theta_1 + \omega L_u\cos\theta_1\right)^2}{Z_u} \qquad \text{(AI.2)}$$

where $Z_u = 1/Y_u$ is the impedance of the shunt branch, which nulls at ω_0. Since both the numerator and the denominator of (AI.2) are zero in the indicated limit, it is necessary to apply the L'Hôpital rule. However, for simplicity, let us take the derivatives with θ_1, rather than with the angular frequency, that is

$$\lim_{\theta_1\to\theta_{1,0}}\frac{2\left(Z_1\sin\theta_1 + \omega L_u\cos\theta_1\right)\left[\left(Z_1 + \frac{L_u v_p}{l_1}\right)\cos\theta_1 - L_u\frac{\theta_1 v_p}{l_1}\sin\theta_1\right]}{Z_u'} \qquad \text{(AI.3)}$$

where $\theta_{1,0}$ is the electrical length of the lines at ω_0, v_p is the phase velocity of the lines, l_1 is their physical length, and Z_u' is the derivative of the shunt impedance with θ_1 (proportional to the derivative with ω). Inspection of (AI.3) reveals that the numerator is null since the left-hand term is null (condition 9), whereas the right-hand term is finite. However, the denominator is finite, as corresponds to the derivative of any reactance with frequency at resonance. Therefore, the previous limit is null, and hence $B_u = 0$.

For which concerns D, the numerator of (7), it can be expressed as follows:

$$D_u = 1 - \frac{2\sin\theta_1}{Z_1}\left(\omega L_u\cos\theta_1 + Z_1\sin\theta_1\right) + \\ + jY_u\left(\omega L_u\cos\theta_1 + Z_1\sin\theta_1\right)\left(\cos\theta_1 + \frac{\omega L_u\sin\theta_1}{Z_1}\right) \qquad \text{(AI.4)}$$

According to the previous equation, if (9) is satisfied, the second term is null. The third term is also null, unless $Y_u \to \infty$. Hence, if Y_u is finite, $D_u = 1$, I_2 given by (11) is not null, and therefore a transmission zero does not occur (as one expects since a transmission zero requires that $Y_u \to \infty$). If $Y_u \to \infty$, the third term in (AI.4) is neither null nor infinite, but finite. The reason is that, in this case, application of the L'Hôpital rule, by considering $Z_u = 1/Y_u$, provides a finite value of both the numerator and the denominator. According to these words, if follows that $D \neq 1$.

APPENDIX II

By excluding the shunt reactance of the upper branch in the circuit of Fig. 1(b), the elements of the *ABCD* matrix can be calculated. In particular, the diagonal elements are given by

$$A = D = \cos^2\theta_1 - \sin^2\theta_1 - \frac{2\omega_0 L_u\sin\theta_1\cos\theta_1}{Z_1} \qquad \text{(AII.1)}$$

Since the electrical length, ϕ, of the unit cell of a periodic structure in the allowed bands is given by [23]

$$\cos\phi = \frac{A+D}{2}\ , \qquad \text{(AII.2)}$$

by forcing $\phi = 2\pi$, it follows that $A = 1$, which is equivalent to (9).

REFERENCES

[1] T. Driscoll, G.O. Andreev, D.N. Basov, S. Palit, S.Y. Cho, N.M. Jokerst, and D.R. Smith, "Tuned permeability in terahertz split ring resonators for devices and sensors," *Appl. Phys. Lett*., vol 91, paper 062511-1-3, 2007.

[2] R. Melik, E. Unal, N.K. Perkgoz, C. Puttlitz, and H.V. Demir, "Metamaterial-based wíreles strain sensors," *Appl. Phys. Lett*., vol. 95, paper 011106-1-3, 2009.

[3] R.A. Yogi, R.S. Parolia, R.N. Karekar, and R.C. Aiyer, "Microwave microstrip ring resonador as a paper moisture sensor: study with different grammage," *Meas. Sci. Technol*. vol *13*, pp. 1558−1562, 2002.

[4] X-J. He, Y. Wang, J-M. Wang, and T-L. Gui, "Thin film sensor based tip-shaped splits ring resonator metamaterial for microwave application," *Microsystems Technology*, vol. 16, pp. 1735−1739, 2010.

[5] M. S. Boybay and O. M. Ramahi, "Material characterization using complementary split-ring resonators," *IEEE Trans. Instrum. Meas*., vol. 61, no. 11, pp. 3039−3046, Nov. 2012.

[6] C.-S. Lee and C.-L. Yang, "Complementary split-ring resonators for measuring dielectric constants and loss tangents," *IEEE Microw. Wireless Compon. Lett.*, vol. 24, no. 8, pp. 563−565, Aug. 2014.

[7] C.-L. Yang, C.-S. Lee, K.-W. Chen, and K.-Z. Chen, "Noncontact measurement of complex permittivity and thickness by using planar resonators," *IEEE Trans. Microw. Theory Techn.*, vol. 64, no.1, pp. 247−257, Jan. 2016.

[8] M. Puentes, C. Weiß, M. Schüßler, and R. Jakoby, "Sensor array based on split ring resonators for analysis of organic tissues," in *IEEE MTT-S Int. Microw. Symp.*, Baltimore, MD, USA, Jun. 2011, pp. 1−4.
[9] M. Puentes, *Planar Metamaterial Based Microwave Sensor Arrays for Biomedical Analysis and Treatment*. Springer, Heidelberg, Germany, 2014.
[10] T. Chretiennot, D. Dubuc, and K. Grenier, "A microwave and microfluidic planar resonator for efficient and accurate complex permittivity characterization of aqueous solutions," *IEEE Trans. Microw. Theory Techn.*, vol. 61, no. 2, pp. 972−978, Feb. 2013.
[11] A. Abduljabar, D. Rowe, A. Porch, and D. Barrow, "Novel microwave microuidic sensor using a microstrip split-ring resonator," *IEEE Trans. Microw. Theory Techn*., vol. 62, no. 3, pp. 679−688, Mar. 2014.
[12] A. Ebrahimi, W. Withayachumnankul, S. Al-Sarawi, D. Abbott, "High-sensitivity metamaterial-inspired sensor for microfluidic dielectric characterization," *IEEE Sensors J.*, vol. 14, no. 5, pp. 1345−1351, May 2014.
[13] W. Withayachumnankul, K. Jaruwongrungsee, A. Tuantranont, C. Fumeaux, and D. Abbott, "Metamaterial-based microfluidic sensor for dielectric characterization," *Sensor Actuat. A Phys.*, vol. 189, pp. 233−237, Jan. 2013
[14] H.-J. Lee and J.-G. Yook, "Biosensing using split-ring resonators at microwave regime," *App. Phys. Lett*., vol. 92, no. 25, p. 254103, 2008.
[15] E. Ekmekci and G. Turhan-Sayan, "Multi-functional metamaterial sensor based on a broad-side coupled SRR topology with a multi-layer substrate," *App. Phys. A* , vol. 110, no. 1, pp. 189−197, Jan. 2013.
[16] C. Damm, M. Schussler, M. Puentes, H. Maune, M. Maasch, and R. Jakoby, "Artificial transmission lines for high sensitive microwave sensors," *IEEE Sensors Conf.,* Christchurch, New Zealand, pp. 755−758, Oct. 2009.
[17] C. Damm, *Artificial Transmission Line Structures for Tunable Microwave Components and Microwave Sensors*, Shaker Verlag, Aachen, Germany, 2011.
[18] M. Schueler, C. Mandel, M. Puentes, and R. Jakoby, "Metamaterial inspired microwave sensors," *IEEE Microw. Mag.*, vol. 13, no. 2, pp. 57–68, Mar. 2012.
[19] M. Tiuri, "Microwave Sensor Applications in Industry," in *Europ. Microw. Conf.*, pp. 25−32, Sep. 1987.
[20] J. G. Webster, *The Measurement Instrumentation and Sensors Handbook*. Boca Raton, FL, USA: CRC, 1999.
[21] J. Fraden, *Handbook of Modern Sensors: Physics, Design, and Applications*, 3rd ed. New York, NY, USA, Springer, 2004.
[22] J. Naqui, M. Durán-Sindreu and F. Martín, "Novel Sensors Based on the Symmetry Properties of Split Ring Resonators (SRRs)," *Sensors*, vol 11, pp. 7545−7553, 2011.
[23] F. Martín, *Artificial Transmission Lines for RF and Microwave Applications*, John Wiley, Hoboken, NJ, 2015.
[24] J. Naqui, *Symmetry properties in transmission lines loaded with electrically small resonators: circuit modeling and applications*, Springer, Heidelberg, Germany, 2016.
[25] J. Naqui, M. Durán-Sindreu, and F. Martín, "Alignment and Position Sensors Based on Split Ring Resonators," *Sensors*, vol. 12, pp. 11790−11797, 2012.
[26] A.K. Horestani, C. Fumeaux, S.F. Al-Sarawi, and D. Abbott, "Displacement sensor based on diamond-shaped tapered split ring resonator," *IEEE Sens. J.*, vol. 13, pp. 1153–1160, 2013.
[27] A.K. Horestani, D. Abbott, and C. Fumeaux, "Rotation sensor based on horn-shaped split ring resonator," *IEEE Sens. J.*, vol. 13, pp. 3014–3015, 2013.
[28] J. Naqui and F. Martín, "Transmission Lines Loaded with Bisymmetric Resonators and Their Application to Angular Displacement and Velocity Sensors," *IEEE Trans. Microw. Theory Techn*., vol. 61, no. 12, pp. 4700–4713, Dec. 2013.
[29] J. Naqui and F. Martín, "Angular displacement and velocity sensors based on electric-LC (ELC) loaded microstrip lines," *IEEE Sensors J.*, vol. 14, no. 4, pp. 939–940, Apr. 2014.
[30] A.K. Horestani, J. Naqui, D. Abbott, C. Fumeaux, and F. Martín, "Two-dimensional displacement and alignment sensor based on reflection coefficients of open microstrip lines loaded with split ring resonators," *Elec. Lett.*, vol. 50, pp. 620–622, Apr. 2014.
[31] J. Naqui and F. Martín, "Microwave sensors based on symmetry properties of resonator-loaded transmission lines: a review," *Journal of Sensors*, vol. 2015, Article ID 741853, 10 pages, 2015.
[32] J. Naqui, J. Coromina, A. Karami-Horestani, C. Fumeaux, and F. Martín, "Angular displacement and velocity sensors based on coplanar waveguides (CPWs) loaded with S-shaped split ring resonator (S-SRR)," *Sensors*, vol. 15, pp. 9628–9650, 2015.
[33] A. K. Horestani, J. Naqui, Z. Shaterian, D. Abbott, C. Fumeaux, and F. Martín, "Two-Dimensional Alignment and Displacement Sensor based on Movable Broadside-coupled Split Ring Resonators," *Sensors and Actuators A*, vol. 210, pp. 18–24, April 2014.
[34] J. Naqui, C. Damm, A. Wiens, R. Jakoby, L. Su, and F. Martín, "Transmission lines loaded with pairs of magnetically coupled stepped impedance resonators (SIRs): modeling and application to microwave sensors," *IEEE MTT-S Int. Microwave Symp*., Tampa, FL, USA, June 2014, pp. 1–4.
[35] L. Su, J. Naqui, J. Mata-Contreras, and F. Martín "Modeling metamaterial transmission lines loaded with pairs of coupled split ring resonators," *IEEE Ant. Wireless Propag. Lett.*, vol. 14, pp. 68–71, 2015.
[36] L. Su, J. Naqui, J. Mata, and F. Martín, "Dual-band epsilon-negative (ENG) transmission line metamaterials based on microstrip lines loaded with pairs of coupled complementary split ring resonators (CSRRs): modeling, analysis and applications," *9th International Congress on Advanced Electromagnetic Materials in Microwaves and Optics*, Metamaterials 2015, Oxford, UK, Sep., 7-12, 2015.
[37] L. Su, J. Naqui, J. Mata-Contreras, P. Vélez, and F. Martín, "Transmission line metamaterials based on pairs of coupled split ring resonators (SRRs) and complementary split ring resonators (CSRR): a comparison to the light of the lumped element equivalent circuits," *International Conference on Electromagnetics for Advanced Applications*, ICEAA 2015, Torino, Italy, 7-11 Sep. 2015.
[38] L. Su, J. Naqui, J. Mata-Contreras, and F. Martín, "Modeling and applications of metamaterial transmission lines loaded with pairs of coupled complementary split ring resonators (CSRRs)," *IEEE Ant. Wireless Propag. Lett.*, vol. 15, pp. 154–157, 2016.
[39] L. Su, J. Naqui, J. Mata-Contreras, and F. Martín, "Cascaded Splitter/Combiner Microstrip Sections Loaded with Complementary Split Ring Resonators (CSRRs): Modeling, Analysis and Applications," *IEEE MTT-S Int. Microwave Symp.* (IMS'16), San Francisco, CA, USA, May 2016, pp. 1–4.
[40] J. Naqui, C. Damm, A. Wiens, R. Jakoby, L. Su, and F. Martín, "Transmission Lines Loaded with Pairs of Stepped Impedance Resonators: Modeling and Application to Differential Permittivity Measurements," *IEEE Trans. Microw. Theory Techn*., published online, DOI: 10.1109/TMTT.2016.2610423.
[41] J.D. Baena, J. Bonache, F. Martín, R. Marqués, F. Falcone, T. Lopetegi, M.A.G. Laso, J. García, I Gil, M. Flores-Portillo and M. Sorolla, "Equivalent circuit models for split ring resonators and complementary split rings resonators coupled to planar transmission lines," *IEEE Trans. Microw. Theory Techn.*, vol. 53, no. 4, pp. 1451−1461, Apr. 2005.
[42] D.M. Pozar, *Microwave Engineering*, 3rd ed. John Wiley, Hoboken, NJ, USA, 2005.
[43] J. Bonache, M. Gil, I. Gil, J. Garcia-García, and F. Martín, "On the electrical characteristics of complementary metamaterial resonators," *IEEE Microw. Wireless Compon. Lett.*, vol. 16, no. 10, pp. 543−545, Oct. 2006.

Lijuan Su (S'15) was born in Qianjiang, Hubei, China, in 1983. She received the Bachelor's degree in Communication Engineering and the M.E. degree in Circuits and Systems from Wuhan University of Technology, Wuhan, China, in 2005 and 2013, respectively. She is currently pursuing the Ph.D. degree in metamaterials applied to RF/microwave sensors at the Universitat Autonoma de Barcelona, Barcelona, Spain.

From 2005 to 2009, she was an Engineer with China Telecom Corporation Ltd.

Javier Mata-Contreras was born in 1976 in Málaga (Spain). He received the Ingeniería de Telecomunicación Degree from the Universidad de Málaga (UMA) in 2000 and the PhD degree from the same university in 2010, with the Thesis "Distributed Amplifiers and Mixers with Transmission Lines based on Metamaterials".

In 2000, he joined the UMA Department of Ingeniería de Comunicaciones UMA as Assistant Professor. He is currently working at CIMITEC and the Universitat Autònoma de Barcelona as Visitant Professor. His research interests include active and

passive microwave devices and active distributed circuits based on metamaterials, among others.

Paris Vélez (S'10-M'14) was born in Barcelona (Spain) in 1982. He received the degree in Telecommunications Engineering, specializing in Electronics in 2008 and the Electronics Engineering degree in 2010 from the Universitat Autònoma de Barcelona. In 2014 he received his PhD in Electrical Engineering from the UAB with a thesis entitled "Common mode suppression differential microwave circuits based on Metamaterial concepts and semilumped resonators". During the PhD he was awarded with a predoctoral teaching and research fellowship by the Spanish Government from 2011 to 2014.
Dr. Vélez is a reviewer of the IEEE T-MTT and of other journals. Actually, his scientific activity is focused on the miniaturization of passive circuits RF / microwave and sensors based Metamaterials. He is currently working in subjects related to Metamaterials sensors for fluidics detection at LAAS-CNRS through TECNIOSpring fellowship cofounded by Mari Curie program.

Ferran Martín (M'04-SM'08-F'12) was born in Barakaldo, Vizcaya, Spain, in 1965. He received the B.S. Degree in Physics from the Universitat Autònoma de Barcelona (UAB) in 1988 and the PhD degree in 1992.
From 1994 to 2006, he was Associate Professor in Electronics at the Departament d'Enginyeria Electrònica (Universitat Autònoma de Barcelona), and since 2007 he is Full Professor of Electronics. In recent years, he has been involved in different research activities including modelling and simulation of electron devices for high frequency applications, millimeter wave and THz generation systems, and the application of electromagnetic bandgaps to microwave and millimeter wave circuits. He is now very active in the field of metamaterials and their application to the miniaturization and optimization of microwave circuits and antennas. He is the head of the Microwave Engineering, Metamaterials and Antennas Group (GEMMA Group) at UAB, and director of CIMITEC, a research Center on Metamaterials supported by TECNIO (Generalitat de Catalunya). He has organized several international events related to metamaterials, including Workshops at the IEEE International Microwave Symposium (years 2005 and 2007) and European Microwave Conference (2009), and the Fifth International Congress on Advanced Electromagnetic Materials in Microwaves and Optics (Metamaterials 2011), where he has acted as chair of the Local Organizing Committee. He has acted as Guest Editor for three Special Issues on Metamaterials in three International Journals. He has authored and co-authored over 500 technical conference, letter, journal papers and book chapters, he is co-author of the book on Metamaterials entitled *Metamaterials with Negative Parameters: Theory, Design and Microwave Applications* (John Wiley & Sons Inc. 2008), author of the book *Artificial Transmission Lines for RF and Microwave Applications* (John Wiley & Sons Inc. 2015), and he has generated 15 PhDs. Ferran Martín has filed several patents on metamaterials and has headed several Development Contracts.
Prof. Martín is a member of the IEEE Microwave Theory and Techniques Society (IEEE MTT-S). He is reviewer of the IEEE Transactions on Microwave Theory and Techniques and IEEE Microwave and Wireless Components Letters, among many other journals, and he serves as member of the Editorial Board of IET Microwaves, Antennas and Propagation and International Journal of RF and Microwave Computer-Aided Engineering. He is also a member of the Technical Committees of the European Microwave Conference (EuMC) and International Congress on Advanced Electromagnetic Materials in Microwaves and Optics (Metamaterials). Among his distinctions, Ferran Martín has received the 2006 Duran Farell Prize for Technological Research, he holds the *Parc de Recerca UAB – Santander* Technology Transfer Chair, he has been the recipient of two ICREA ACADEMIA Awards (calls 2008 and 2013) and recipient of the Ingeniero Comerma Prize in 2015. He is Fellow of the IEEE since 2012 and Fellow of the IET since 2016.